



Seismic response investigation and analytical model of light polymer material-filled CFS shear walls

Wanqian Wang¹ · Jingfeng Wang^{1,2} · Lei Guo¹ · Qihan Shen¹

Received: 4 January 2020 / Revised: 25 March 2020 / Accepted: 28 April 2020 / Published online: 20 May 2020
© Wrocław University of Science and Technology 2020

Abstract

The light polymer material (LPM), prepared with suitable mix proportion and physical method, is a type of low-carbon and environmental-friendly material. Recently, the LPM is developed as structural material for cold-formed steel (CFS) structures to cover the shortages of traditional CFS shear wall. In this paper, material properties of gypsum-based and cement-based LPM including compressive strength, elastic modulus and thermal property were explored by tests. Experimental results demonstrate that LPM exhibits excellent thermal insulation, and the thermal insulation and compressive strength of LPM satisfy the demand of bearing capacity and thermal insulation property of shear walls. To explore the effect of LPM on seismic response and failure modes of CFS shear walls, three specimens are manufactured and tested under cyclic loading. The existence of LPM in CFS shear wall would restrain the failure of wall studs to some extent. Due to the restriction effect of LPM on wall studs and self-drilling screws and the bond-slip performance between LPM and studs, the shear walls exhibit better seismic behavior than traditional CFS shear walls. At last, a modified equivalent bracing model is employed to predict the lateral stiffness of LPM-filled CFS shear walls considering the effect of filling materials, rib lath, and sheathing. The lateral stiffness obtained by the proposed method is compared to the experimental results in this paper and other researches, and the proposed model is proved to supply a conservative result which is safe to be adopted in the design and application of the LPM-filled CFS shear wall.

Keywords Light polymer material (LPM) · Material properties · Cold-formed steel (CFS) shear wall · Seismic response · Modified equivalent bracing model

List of symbols

CFS	Cold-formed steel	i_1	Linear stiffness of end stud
EPS	Expanded polystyrene	f'_c	Cylinder compressive strength
LPM	Light polymer material	a_s	Horizontal length of the compression zone
Q_{BA} & Q_{DC}	Shearing forces of the end stud base	a_w	Uniform width of diagonal rod as a prismatic form
n	Number of wall stud	A_w	Cross-sectional area of the LPM
N_{BC}	Compression of rod BC	$E_{sm}A_{sm}$	Axial rigidity of the diagonal rod
N_{ri}	Axial force of diagonal rod	G_s	Shear modulus of wall panel
N_{sm}	Axial force of diagonal rod	t_s	Thickness of the wall panel
Δ	Lateral deformation of shear wall top	S_0	Deformation of the self-drilling screws connection
A_f	Cross-section area of equivalent compressive rod	F_s	Strength of self-drilling screws connection
E_f	Elastic modulus of LPM	n_s	Screw number along the vertical edge on one side of the wall
		$E_{ri}A_{ri}$	Axial rigidity of the diagonal rod

✉ Jingfeng Wang
jfwang008@163.com

¹ School of Civil Engineering, Hefei University of Technology, Hefei 230009, Anhui Province, China

² Anhui Key Laboratory of Civil Engineering Structures and Materials, Hefei 230009, Anhui Province, China

1 Introduction

With the advancement of green buildings and promotion of new countryside construction, environment-friendly and energy-saving materials come to the spotlight. According to the recent statistics [1], plenty of expanded polystyrene (EPS) has a great negative impact on the ecological environment in the world. Moreover, comprehensive statistics above show that the output of desulfurization gypsum from power, heat and supply industries are approximately 66.437 million tons, of which more than 12 million tons are not comprehensively utilized. The industrial wasting gypsum not only occupies large amount of land resources, but also causes great harm to the natural environment through long-term accumulation. Therefore, it is necessary to broaden the utilization ways of solid waste desulfurization gypsum and EPS. Since the EPS has the characteristics of light bulk density, good crack resistance, excellent thermal insulation, low moisture absorption and good stability [2], it may be employed in building structures. In recent years, EPS [3, 4] has already been adopted as an ingredient in different building materials. Joseph [3] and Mousavi [4] employ the EPS as composing materials of concrete, which are, respectively, used in sandwich panels and super-lightweight shear walls. And the industrial waste flue gas desulfurization gypsum is also utilized in cement as building materials, such as Wu [5] and Zhang [6]. The researches indicated the two types of wasting materials would presumably be used as building materials in the future and the pollution caused by them would be significantly reduced.

Against the above background, a new type of light polymer material (LPM) is proposed in this study adopting EPS and desulfurization gypsum as main ingredients. Meanwhile, another type of LPM is prepared using EPS and cement as main ingredients. They are, respectively, defined as gypsum-based LPM and cement-based LPM for distinguish. Furthermore, the LPM exhibits lower density (less than 500 kg/m^3), lower self-weight, better fire resistance, sound insulation characteristics and thermal insulating property (with the thermal conductivity less than $0.06 \text{ W/(m}^2 \text{ K)}$). Therefore, the LPM can make full use of the waste, protect the environment and satisfy the requirement of “green development” for construction industry. Additionally, the LPM can reduce the self-weight of structural components, and then decreases earthquake damages of the whole structures.

Due to the specific merits of LPM mentioned above, the LPM was applied as filling materials in the cold-formed steel (CFS) structures. Thus, a novel type of CFS structure using LPM-filled CFS shear wall (as shown in Fig. 1) was proposed. The application of LPM satisfied

the needs of environmental-friendly and energy-saving performance for green buildings. Besides, the filled CFS shear wall can overcome the shortcomings, such as sound insulation performance and fire resistance, of conventional CFS shear walls. In addition, this novel composite wall has been used in low- and multi-rise residential and office buildings in Anhui province, China, as shown in Fig. 1. Until now, the previously published papers mainly investigated the performance of conventional CFS shear walls. The compressive behavior [7], cyclic behavior [8], fire performance [9], dynamic response [10] and design method [11] of CFS shear walls have been explored. Specially, Wang [12] conducted the cyclic test and numerical analytical assessment of CFS steel shear walls using tube truss. Apart from these abovementioned works, different types of filling materials are adopted in CFS shear walls to promote the performance. The material using in the CFS shear wall mainly include lightweight mortar [13], lightweight concrete [14], lightweight foamed concrete [15], high-strength lightweight foamed concrete [16] and lightweight flue gas desulfurization gypsum [17]. Nevertheless, available literatures concerning this type of LPM-filled CFS shear wall and the effect of LPM on the CFS shear wall can rarely be found.

In this study, LPM was prepared by using suitable mixes and proportion. Material properties of gypsum-based and cement-based LPM including compressive strength, elastic modulus and thermal property were explored by tests. To explore the effect of LPM on CFS shear walls, a pure CFS framing wall without filling and two LPM-filled CFS shear walls were manufactured and tested under cyclic loading. The effect of LPM on the failure patterns, hysteretic behavior, mechanical behaviors and energy dissipation capacity was studied. Follow it, a modified equivalent bracing model is proposed to predict the lateral stiffness of shear wall in considering the filling material, wall panel and rib lath. Consequently, the results in this paper provide a reference to design and apply the novel LPM-filled CFS shear wall.

2 Light polymer material

2.1 Materials and mixture proportion

In this paper, light polymer materials are divided into gypsum-based and cement-based materials according to different cementitious materials. The fundamental properties of LPM are listed in Table 1. The gypsum-based LPM is produced incorporating the gypsum, retardants, expanded polystyrene (EPS), additives and water. Polystyrene beads with average diameter, bulk density and specific gravity of 6.5 mm, 16.6 kg/m^3 and 0.016, respectively, were used as lightweight aggregate. In attempt to postpone fast setting



Fig. 1 Application of LPM-filled CFS wall in building

Table 1 Mix proportion of LPM

LPM	Cement (kg/m ³)	Fly ash (kg/m ³)	Gypsum (kg/m ³)	Retarder (kg/m ³)	Expansive agent (kg/m ³)	Additive (kg/m ³)	EPS (m ³)	Water (kg/m ³)
Cement-based	300	65	–	–	125	2	0.6	225
Gypsum-based	–	–	450	2.0	–	2.0	0.75	275

time of the gypsum-based LPM, the retarders are added into the gypsum-based LPM. The gypsum retarder used in this paper was sodium polyphosphate.

The cement-based LPM is prepared using the cement, fly ash, expanded polystyrene, expansive agent, additives and

water. Ordinary Portland cement and fly ash are employed as admixtures to improve the workability, enhance long-term strength and cut cost [18]. The using of expansive agent can improve the crack resistance of LPM notably. The expansive agent used in this paper was calcium sulfoaluminate.

Additionally, the density and compressive strength of the LPM can be changed by varying the mixing amount of the light admixture.

The LPM specimens were cast to investigate the various performance parameters. Three cubes of $100 \times 100 \times 100$ (mm), three prisms of $100 \times 100 \times 300$ (mm) and three plate of $300 \times 300 \times 30$ (mm) were casted for each type of LPMs. All specimens were kept at temperatures of $20 (\pm 5) ^\circ\text{C}$ and had the knockout time of $24 (\pm 2)$ h from completion of the pouring. Then, the specimens were kept in standard curing condition, which had the temperatures of $20 (\pm 2) ^\circ\text{C}$ and the relative humidity more than 90%, until the day of testing. The compressive strength and elastic modulus of specimens were measured at 28 days in accordance with JGJ/T 70 [19]. The plate specimens were used to measure the thermal conductivity based on GB/T 10294 [20].

2.2 Properties of LPM knockout time of

2.2.1 Compressive strength

For each type of LPM (including gypsum-based and cement-based), three cubic specimens for compressive test are employed. The dry densities of gypsum-based and cement-based are, respectively, 449 kg/m^3 and 456 kg/m^3 . Currently, there are no relevant regulations for LPM; so the test of LPM is conducted as per JG/T 266 [21]. The compressive strength of LPM is evaluated after 28 days at the loading rate of 0.1 kN/s . The photograph of test setup is shown in Fig. 2a. The measured average compressive strength of gypsum- and cement-based is 1.1 MPa and 2.1 MPa , respectively. The results demonstrated that the compressive strength of cement-based LPM is almost 1.9 times higher than that of gypsum-based LPM. In addition, the splitting tensile strength of LPM is calculated based on the empirical

formulas showed by the previous experimental studies [22, 23], which present an obvious relationship between tensile and compressive strength.

2.2.2 Elastic modulus

For each type of LPM (including gypsum-based and cement-based), three prism specimens for compressive test are adopted. The elastic modulus of different LPM types is obtained by the method proposed in standards GB/T 50081 [24] and JG/T 266 [21]. The test photograph is shown in Fig. 2b, and stress–strain curve of each prism specimen is shown in Fig. 3. Based on the stress (σ)- strain (ϵ) curves, the elastic modulus of gypsum-based and cement-based LPM is obtained, the value of which are, respectively, 200 MPa and 250 MPa . Moreover, the stress–strain curves for gypsum-based and cement-based LPM are basically linear at the initial loading stage. After the linear stage, the curves of gypsum-based LPM growing slowly, while the curves of gypsum-based LPM exhibit a slight descent, which may be explained as the brittle failure for specimens. A small number of air voids in LPM caused by expansive agent can easily break and decrease the compressive strength.

2.2.3 Thermal property

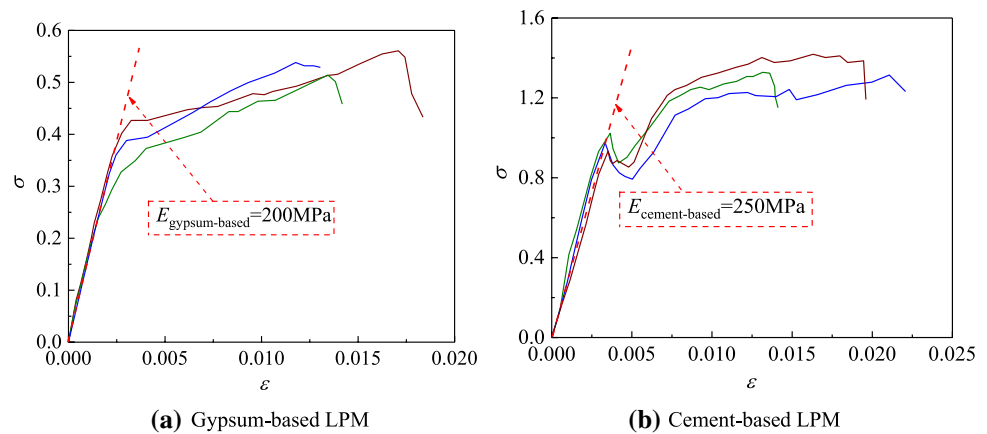
For each type of LPM (including gypsum-based and cement-based), three plate specimens for each type of thermal conductivity are adopted, and the test photograph is shown in Fig. 2 (c). The thermal conductivity of gypsum-based and cement-based was $0.053 \text{ W}/(\text{m}^2.\text{K})$ and $0.051 \text{ W}/(\text{m}^2.\text{K})$, respectively, with corresponding standard deviations of 0.03 and 0.02. Compared with other light materials utilized in CFS shear walls such as foamed concrete [11, 25], the LPM appears better thermal properties. In accordance with the

Fig. 2 Experimental photographs of LPM



(a) Cube compressive strength **(b)** Prism compressive strength **(c)** Thermal conductivity

Fig. 3 Prism-compressive stress–strain curves and elastic modulus of LPM



comparison, the gypsum-based and cement-based LPMs are suitable materials and can be applied as a structural bearing and insulation material in green building.

3 Methodology

3.1 Design of the specimens

In order to investigate the seismic response of LPM-filled CFS shear wall and the effect of LPM on the seismic performance of shear wall, three specimens were fabricated and designated by CFS1, LPM-CFS2 and LPM-CFS3. The specimen CFS1 without filling material was designed as a benchmark. The conventional filling materials mainly functioned as thermal insulation and appeared few effects on the mechanical behaviors of CFS shear wall. Thus, the conventional filling materials are usually neglected in the studies on the mechanical behaviors of CFS shear wall, such as Mohebbi [26] and Pan [27]. Gypsum-based LPM and cement-based LPM were, respectively, used in specimens LPM-CFS2 and LPM-CFS3. The two specimens were compared with specimen CFS1 to study whether this filling material could improve the performance of CFS framing.

The test specimens originated from a two-story building, as shown in Fig. 1. The detail information of all specimens is illustrated in Fig. 4. All specimens are rectangular with a height of 2755 mm and width of 3000 mm. According to specification JGJ 227 [28] and AISI S213 [29], each CFS framing consisted of interior studs, end studs, tracks and horizontal bracing. The wall studs were spaced at 600 mm on center. The CFS framings consist of identical C-section with dimension 89 mm × 41 mm × 11 mm × 0.9 mm, as shown in Fig. 4. To ensure the homogeneity of LPM density over wall specimens, the specimens were fabricated by spraying the LPM on a single-side panel instead of spraying the LPM into the shear wall from the top track with pre-punched holes.

This way of pouring LPM can ensure the achieved densities of formed LPM in the range of $\pm 50 \text{ kg/m}^3$.

In accordance with specification GB/T 15856 [30], CFS components were connected by ST4.8-grade ($d=4.8 \text{ mm}$) self-drilling screws to form CFS framing. Then, single-side wall panel were attached to the framing using ST4.8-grade self-drilling screws spaced at 150 mm and 300 mm. Following it, LPM was sprayed into the cavity of CFS framing as filling material. Finally, rib laths were attached to another side of framing, and the LPM was sprayed on the face of rib laths with a thickness of 25 mm. The whole of the rib lath and the 25-mm-thick LPM were jointly considered as the rib lath sheathing (as shown in Fig. 5) in this paper for convenience.

3.2 Material properties

The CFS framing components are fabricated from the galvanized steel sheets with a nominal yield strength of 550 MPa. The steel coupons are subjected to tensile tests to determine the mechanical properties. The material properties of the steel members are illustrated in Table 2. And the nominal yield strength of the rib laths is 345 MPa.

The elastic modulus and static bending strength of the sheathings are obtained according to GB/T 17657 [31]. The results are listed in Table 3.

3.3 Test setup and loading procedure

The test setup was arranged according to JGJ 227 [28], as presented in Fig. 6. The top and bottom tracks of the CFS framing were connected to the distributive girder and bottom foundation beam with six M16 × 190 mm bolts to facilitate the transfer of a horizontal shear load. The specimens were fastened to the top and bottom through four hold-downs in each wall corner (as shown in Fig. 7). The vertical loads were applied by a 500 kN, and the loads are transmitted uniformly to the specimen with a distributive girder. A

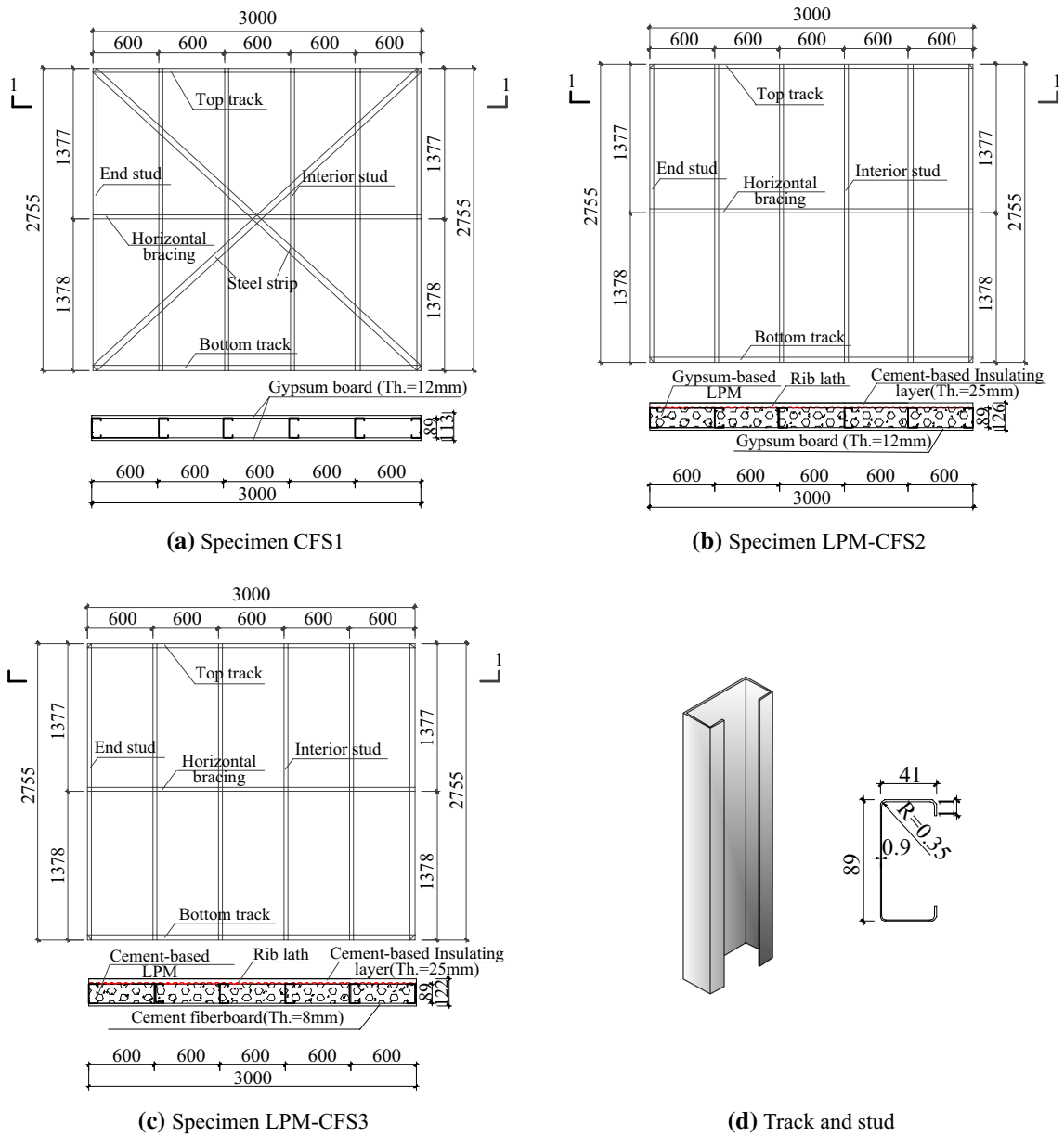


Fig. 4 Detail of specimen dimensions

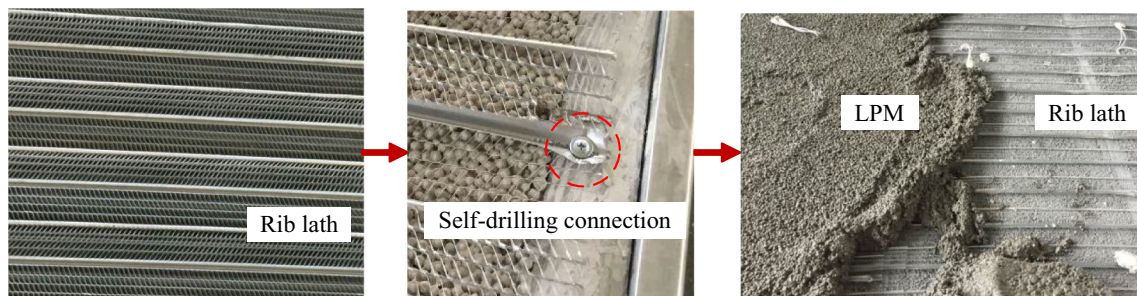


Fig. 5 Configurations of rib lath sheathing

Table 2 Material properties of steel

Thickness <i>t</i> /mm	Elastic modulus <i>E_s</i> /MPa	Yield stress <i>f_y</i> /MPa	Tensile stress <i>f_u</i> /MPa	Elongation <i>δ</i> /%
0.9	2.06×10^5	615	692.5	10.6

Table 3 Material properties of sheathing

Sheathing	Thickness/mm	Static bending strength/MPa	Elastic modulus/ MPa
Gypsum board	12	5.2	1500
Cement fiberboard	8	17.25	5000

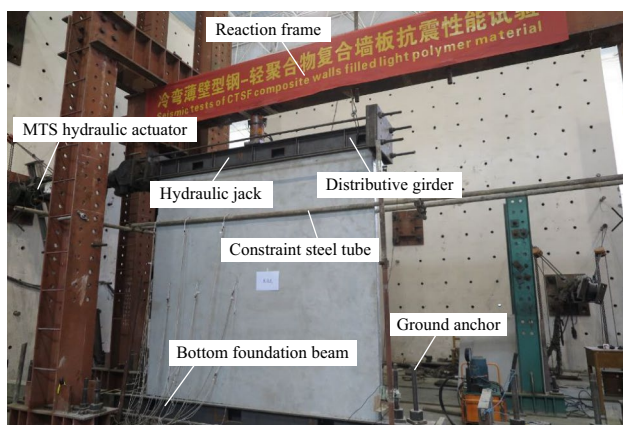


Fig. 6 Test setup

1000kN MTS hydraulic actuator with a displacement range of ± 250 mm was installed to impose the lateral cyclic loads to the specimens. In order to avoid out-plane deformation of

the specimen, two constraint steel tubes were installed on the double side of specimens.

The vertical load imposed to the specimen is obtained by simulating the actual force condition, and the 80kN axial load was an average force in consideration of the dead loads and live loads on this wall. During the tests, the vertical loads remained constant. The lateral cyclic loads are applied to the distributive girder end according to the loading history. Generally, the displacement-controlled load is applied to all test specimens followed the ATC-24 [32], as depicted in Fig. 8. The loading is terminated after the load decreased to 85% of the peak loads or until failure.

4 Experimental results

The influence of LPM on the failure modes and seismic response of CFS shear walls are discussed in this section.

4.1 Observed failure patterns

Figure 9(a) shows the failure modes of specimen CFS1, which indicated that unfilled CFS shear wall failed by local buckling of wall studs and the screw pull-over failure at the sheathing-to-stud connections. Owing to the increasing lateral displacement, the cracking and bulging of gypsum boards occurred and the both-side X-shaped bracings relaxed. In addition, the failure modes of specimen LPM-CFS2 also experienced a typical shear failure with local damage (see Fig. 9(b)). Bond-slip cracks between the LPM and wall studs occurred as the test continued. It should be stressed that the compressive failure caused by the cyclic loading occurred at the corners of the LPM. The relative slippage between the LPM and the wall studs improved the deformation capacity of the walls.

Fig. 7 Configurations of hold down

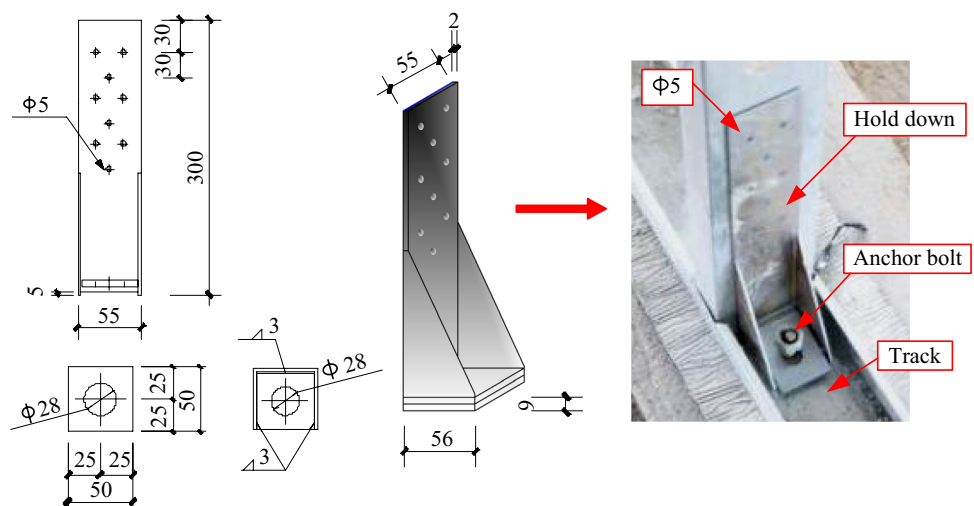
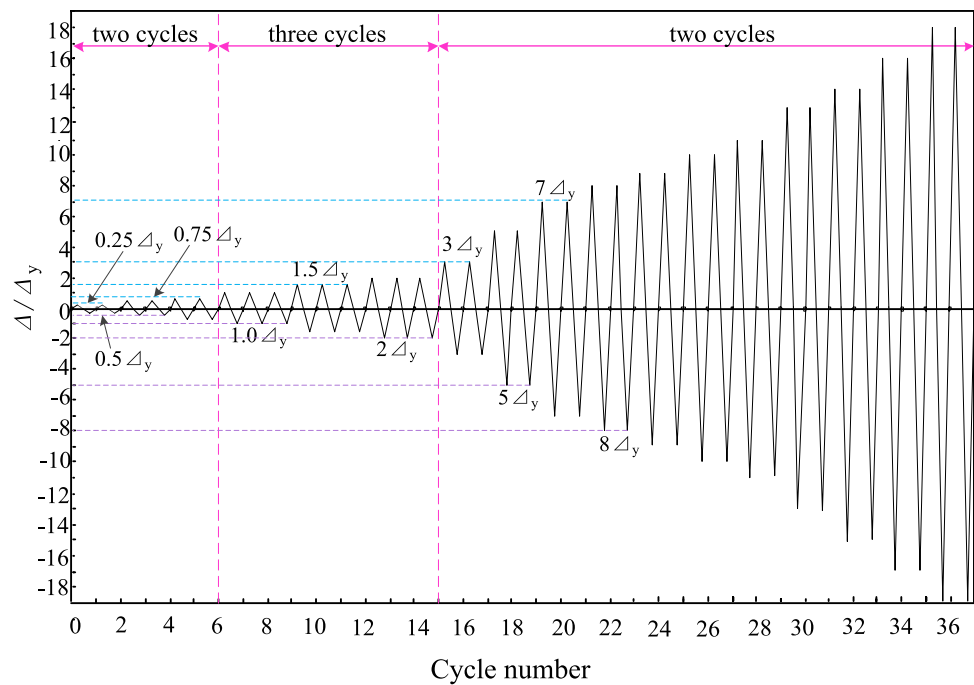


Fig. 8 Loading history



Comparison of the failure modes between specimens CFS1 and LPM-CFS2 showed that the specimen LPM-CFS2 failed with slight local buckling in interior studs, which indicated that LPM had an obvious effect on delaying the wall studs buckling of the CFS framing walls. It attributed to the restriction effect of LPM on the deformation of wall studs. Compared with the specimen CFS1 without filling material, slight bugling appeared on the gypsum board in specimen LPM-CFS1 because of the bonding between LPM and the gypsum board. The restriction effect improved with the compressive strength of LPM increasing. It resulted that no local buckling is observed at the interior studs of specimen LPM-CFS3 with cement-based LPM (Fig. 9(c)). Therefore, the LPM can apparently change the failure modes of CFS shear wall. Over all, in order to make full use of the performance of each component, appropriate failure patterns may be occurred from sheathing cracking to stud buckling to filling materials cracking.

4.2 Effect of LPM on hysteretic and envelop curves

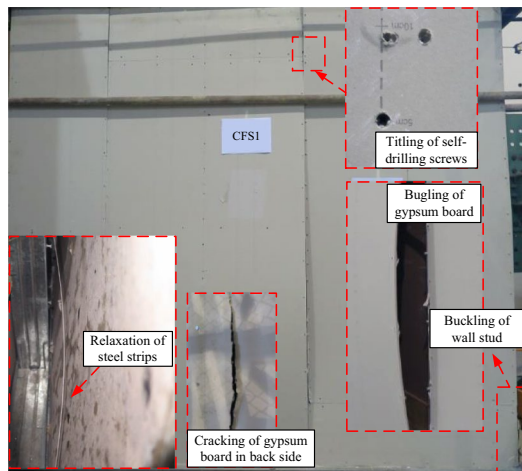
The force–displacement hysteresis curves and envelop curves in Fig. 10 can obviously reflect the cyclic response of the test specimens. The test specimens reached the elastic–plastic stage rapidly after a short elastic stage, and the curves developed gradually from linearity to spindle shape. In addition, the curves displayed residual deformation after unloading. As the load increased, the curves became an arc shaped, accompanied by a certain level of pinching. Thus, the specimens entered the yield stage. When the hysteresis curves changed the shape to a reversed ‘S’ shape,

the pinching level became distinct. As the loading reached the peak point, the curves again changed gradually from a reversed ‘S’ shape to a ‘Z’ shape, which resulted from the spalling of the wall sheathing, buckling of the wall studs and relative slippage between the CFS framing and LPM. And the pinching level became distinct with the further increase in displacement. Beyond the peak loads, significant strength and stiffness degradations occurred due to the buckling of wall studs and crushing of LPM and wall boards. The envelope curves of the test specimens exhibited no apparent yield point since the linear stage was relatively short and the obvious nonlinearity occurred early.

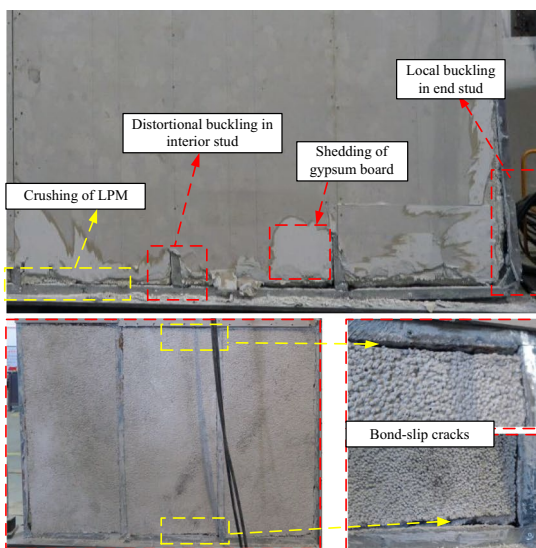
Compared with specimen CFS1 without filling material, specimens LPM-CFS2 and LPM-CFS3 exhibited higher shear bearing capabilities and elastic stiffness. It indicated that the LPM resisted the deformation of the self-drilling screws and studs, and improved the bearing capacities of the studs. Besides, the curve of specimen sprayed with cement-based LPM declined slower than that of gypsum-based LPM specimen. It may be explained by the cement-based LPM appeared better ductility than gypsum-based LPM.

4.3 Effect of LPM on mechanical behavior

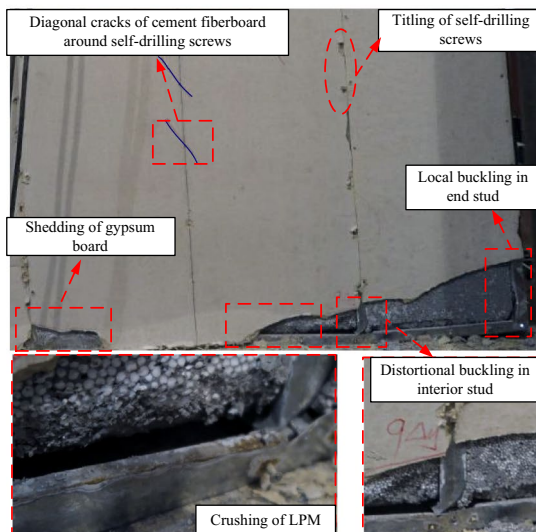
In this paper, the characteristic values were obtained in accordance with JGJ/T 101 [33], as illustrated in Fig. 11. The characteristic values of test specimens are given in Table 4. The test results exhibited that the peak load of CFS shear wall can be increased approximately 2.92–4.31 times by LPM. Compared with specimens LPM-CFS2 and LPM-CFS3, specimen CFS1 appeared a poor lateral bearing



(a) Specimen CFS1



(b) Specimen LPM-CFS2



(c) Specimen LPM-CFS3

Fig. 9 Typical failure modes of specimens

capacity owing to the buckling of the studs without the restrictive effect of the LPM. Additionally, the peak load of the specimen LPM-CFS3 with cement-based LPM was 28% higher than that of specimen LPM-CFS2. The initial stiffnesses of specimens LPM-CFS2 and LPM-CFS3 were, respectively, 2.12 and 3.09 times higher than that of specimen CFS1. This may be explained by the restriction effect of LPM and the certain stiffness of LPM on the CFS framing, which evidently increased the initial stiffness of LPM-filled CFS shear wall. The initial stiffness of the specimen LPM-CFS3 was 31% times higher than that of specimen LPM-CFS2. The results demonstrated that using LPM with higher compressive strength can improve load-bearing capacity and initial stiffness of the wall.

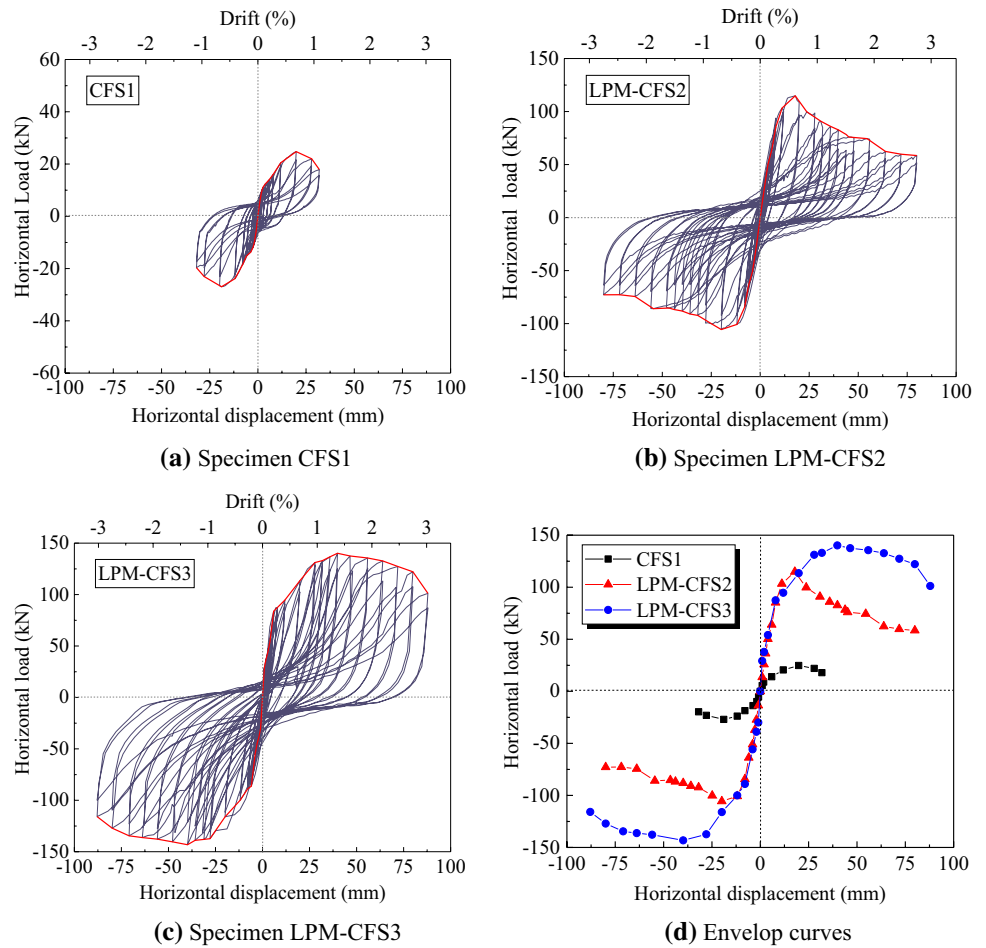
4.4 Effect of LPM energy dissipation capacity

In this paper, the cumulative dissipated energies E were used to assess the energy dissipation capacity of test specimen, and the cumulative dissipated energies in each loading cycle are depicted in Fig. 12. The cumulative dissipated energy of specimens LPM-CFS2 and LPM-CFS3 were, respectively, 2.39 and 27.41 times higher than that of specimen CFS1 in the failure stage. It was benefited from the bond-slip performance between LPM and studs. Evidently, the energy dissipation capacity of specimen LPM-CFS3 was higher than that of specimen LPM-CFS2. This indicated that the bond-slip force between LPM and CFS framing is increased apparently, which can dissipate more seismic energy due to the increase in LPM compressive strength. Consequently, using LPM as filling material contributed to enhance the energy dissipation capacity of the shear walls and keep inelastic deformations before the collapse under earthquake force.

5 Calculation on lateral stiffness

The commonly used model for evaluating the lateral stiffness of CFS shear walls is the equivalent bracing model Ref. [34]. However, the available equivalent bracing model only took the wall studs, self-drilling screws and sheathings into consideration. Therefore, the simplified model is modified in this paper to consider the effect of X-shaped bracing, filling materials and rib lath (as depicted in Fig. 13 and Fig. 14). Assumptions for this model are as follows: (1) the CFS framing is supposed as bar elements that are connected with hinges, and the bases of the end studs are assumed as fixed ends in consideration of the hold-downs; (2) the wall panel is equivalent to a pair of crossed diagonal rods, which only bear the axial load; (3) the filling materials are equivalent to a pair of crossed diagonal rods among the adjacent two studs and horizontal bracing; (4) the rib lath is homogenized so it is assumed as a steel plate.

Fig. 10 Load–displacement hysteretic behaviors of test specimens



Based on the abovementioned assumptions, structural mechanics theories and force-balance principles, the horizontal force in the top of shear wall can be expressed as Eq. (1):

$$P + Q_{BA} + Q_{DC} - 2(n - 1)N_{BC} \cos \alpha - \left(2 \sum_{i=0}^2 N_{ri} + 2 \sum_{m=0}^2 N_{sm} \right) \cos \beta = 0 \tag{1}$$

$$Q_{BA} = Q_{DC} = -\frac{3\Delta i_1}{(H/2)^2} \tag{2}$$

$$\cos \alpha = \frac{l}{\sqrt{l^2 + H^2/4}} \tag{3}$$

$$\cos \beta = \frac{(n - 1)l}{\sqrt{(n - 1)^2 l^2 + H^2}} \tag{4}$$

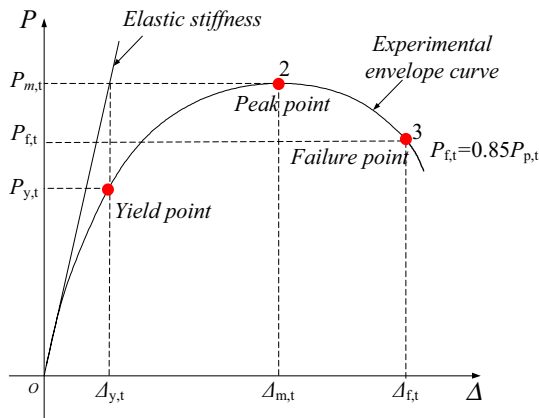


Fig. 11 Definition of characteristic points

where Q_{BA} and Q_{DC} are the shearing forces of the end stud base; n is the number of wall stud; N_{BC} is the compression of rod BC; α and β are depicted in Fig. 13; N_{ri} is the axial force of diagonal rod, which is simplified from the i -side rib laths ($i=0,1,2$); N_{sm} is the axial force of diagonal rod, which is simplified from the m -side wall panels; Δ is the lateral deformation of shear wall top; i_1 is the linear stiffness of end stud.

Table 4 Characteristic values on the load–displacement curves

Specimen	Yielding point		Peak point		Failure point	
	Δ_y/mm	P_y/kN	Δ_m/mm	P_m/kN	Δ_u/mm	P_u/kN
CFS1(+)	3.72	12.28	19.88	24.76	25.87	21.05
CFS1(−)	−3.72	−13.74	−18.87	−26.95	−24.88	−22.92
LPM-CFS2(+)	7.94	87.53	17.89	114.83	26.41	97.61
LPM-CFS2(−)	−7.94	−86.07	−19.87	−105.56	−27.60	−89.73
LPM-CFS3(+)	5.94	83.80	39.87	140.15	80.50	119.13
LPM-CFS3(−)	−5.95	−86.24	−39.87	−143.22	−84.23	−121.74

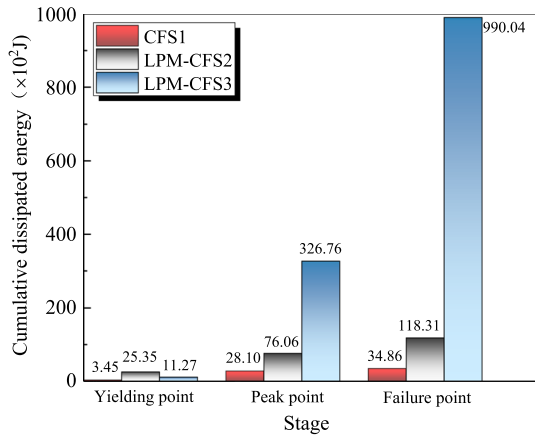


Fig. 12 Cumulative dissipated energy E of test specimens

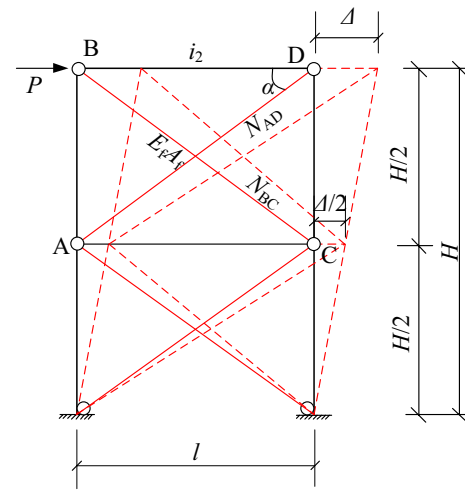


Fig. 14 Calculated substructure of LPM-filled CFS shear wall

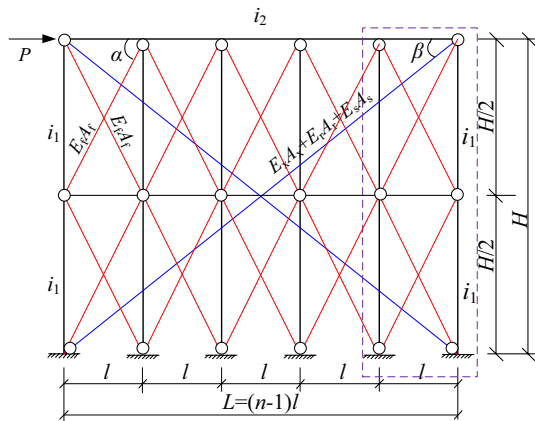


Fig. 13 Modified equivalent bracing model of shear wall

In order to explore the effect of filling materials on lateral stiffness, a calculated substructure (as shown in Fig. 14) was extracted. The LPM of each calculated substructure is divided into two parts, which both have the shear deformation of $\Delta/2$ under the top shear force P . Thus, the LPM is considered as a compressive rod BC and a tension rod AD , and the two rods have identical absolute

values of internal force. The N_{AD} and N_{BC} can be obtained by Eq. (5) according to deformation compatibility.

$$N_{AD} = N_{BC} = \frac{(\Delta/2)E_f A_f}{l^2 + H^2/4} \tag{5}$$

in which, E_f is the elastic modulus of LPM; A_f is the cross-section area of equivalent compressive rod. The cross-section area A_f could be obtained in accordance with Hwang [35–37], and the relevant formulas are expressed as:

$$A_f = a_w \times b_w \tag{6}$$

$$a_w = a_s = \left[0.25 + 0.85 \frac{N}{A_w f'_c} \right] L \tag{7}$$

where f'_c is the cylinder compressive strength; a_s is the horizontal length of the compression zone; a_w is the uniform width of diagonal rod as a prismatic form; A_w is the cross-sectional area of the LPM.

Based on the abovementioned equivalent model, the wall panel can be assumed as two diagonal rods which

have identical absolute values of internal force. The axial force N_{sm} can be calculated by Eq. (8).

$$N_{sm} = \frac{\Delta(n-1)E_{smr}A_{sm}}{(n-1)^2l^2 + H^2} \tag{8}$$

$$E_sA_s = \frac{1}{2} \cdot \frac{[H^2 + (n-1)^2l^2]^{1.5}}{(HL/G_s t_s) + (2S_0/F_s n_s)[H^2 + (n-1)lH]} \tag{9}$$

where $E_{smr}A_{sm}$ is the axial rigidity of the diagonal rod, which was simplified by the m -side wall panels and obtained using Eq. (8) [33, 38]; G_s and t_s are, respectively, the shear modulus and thickness of the wall panel; S_0 is the deformation of the self-drilling screws connection; F_s is the strength of self-drilling screws connection; n_s is the screw number along the vertical edge on one side of the wall. The formulas demonstrate that the self-drilling screws connections are the crucial influencing factor for the contribution provided by wall panels.

At the initial stage, the rib lath tentatively equivalent as a homogeneous steel plate, which can be assumed a wall panel of shear wall. Thus, the axial force N_{ri} can be obtained using Eq. (10-11) referring the calculation of N_{sm} .

$$N_{ri} = \frac{\Delta(n-1)E_{ri}A_{ri}}{(n-1)^2l^2 + H^2} \tag{10}$$

$$E_rA_r = \frac{1}{2} \cdot \frac{[H^2 + (n-1)^2l^2]^{1.5}}{(HL/G_r t_r) + (2S_0/F_r n_r)[H^2 + (n-1)lH]} \tag{11}$$

where $E_{ri}A_{ri}$ is the axial rigidity of the diagonal rod, which was simplified by the i -side rib lath. If the constructions of filling material, X-shaped bracing, rib lath and wall panel for lateral stiffness are considered, the calculation formula of lateral stiffness can be obtained by substituting Eq. (2-11) into Eq. (1), and the formula is expressed as Eq. (12):

$$K = \frac{P}{\Delta} = \frac{24i_1}{H^2} + \frac{(n-1)l^2 E_r A_r}{(l^2 + H^2/4)^{1.5}} + \sum_{i=0}^2 \frac{(n-1)^2 l^2}{(HL/G_{ri} t_{ri}) + (2S_0/F_{ri} n_{ri})[H^2 + (n-1)lH]} + \sum_{m=0}^2 \frac{(n-1)^2 l^2}{(HL/G_{sm} t_{sm}) + (2S_0/F_{sm} n_{sm})[H^2 + (n-1)lH]} \tag{12}$$

The results of the test lateral stiffness and those predicted based on the simplified model are compared in Table 5. The specimens from Ref. [14] and Ref. [15] are also adopted to verified the reliability of Eq. (12) It can be observed that the ratio of K_p to K_t is between 0.62 and 0.82 with the average ratio of 0.72 and the variation of 0.006, indicating that

Table 5 Comparison of lateral stiffness with tests and calculations

Origination	Specimen	K_t (kN/mm)	K_p (kN/mm)	K_p/K_t
This paper	LPM-CFS2	10.93	8.48	0.78
This paper	LPM-CFS3	14.31	11.33	0.79
Ref. [17]	WF1	9.44	6.13	0.65
Ref. [17]	WF3	14.25	10.30	0.72
Ref. [17]	WF5	17.01	10.68	0.63
Ref. [19]	HS-140-3a	3.91	2.42	0.62
Ref. [19]	HS-140-4	4.12	3.37	0.82
Average				0.72
Coefficient of variation				0.006

K_p and K_t are predicted and tested elastic lateral stiffness of CFS shear walls sprayed with LPM, respectively. K_t defines as the average value of positive and negative elastic lateral stiffness in the test

the proposed model can provide a conservative lateral stiffness which is safe in the design. Thus, the results indicated the modified equivalent bracing model can serve as a reliable and relatively conservative prediction method for the elastic lateral stiffness of LPM-filled CFS shear walls. It was notable that the predicted results were about 21% lower than the test results, which may be explained by the stiffness contribution of each component was calculated individually without fully considering the composite actions among the wall studs, sheathings and filling material. Moreover, further researches are still required to confirm the formula for LPM-filled CFS shear wall, because only two shear walls are experimented in this study.

6 Conclusion

The following conclusions could be summarized based on the test and analytical results in this paper:

- (1) Two novel types of LPM were manufactured based on gypsum and cement, respectively. The measured compressive strength of gypsum- and cement-based were, respectively, 1.1 MPa and 2.1 MPa. And the thermal conductivities were all lower than 0.055 W/(m².K). The results indicated that LPMs exhibited certain bearing capacities and significant thermal properties. Therefore, the gypsum-based and cement-based LPM might be suitable materials that could be adopted as structural load-bearing and insulation materials in green buildings.
- (2) The comparative analysis of specimen CFS1 and the other two specimens indicated the using of LPM could restrict the local buckling of wall studs and enhance the self-drilling screw connections. Regarding for the

LPM-filled CFS shear walls, the dominant failure patterns were mainly the local buckling of the end studs, distortion of the interior studs, spalling of the gypsum board or cement fiberboard, titling of self-drilling screws and crushing of the LPM.

- (3) The experimental results confirmed that LPM can significantly improve the seismic responses of CFS framing walls in terms of bearing capacity, stiffness and energy dissipation capacity, which attributed to the bearing capacity of LPM, restriction effect of LPM on the CFS framing, and bond-slip behavior between LPM and CFS framing.
- (4) An equivalent bracing model was modified in this paper to assess the lateral stiffness of LPM-filled CFS shear walls. The proposed model considered the influences of filling material, rib lath and X-shaped bracing. The predicted results have been verified by experimental data in this paper and references. The results demonstrated that the proposed model can predict the lateral stiffness of the LPM-filled CFS shear walls approximatively and safely.

Acknowledgements The research reported in this paper is supported by the National Natural Science Foundation of China (Project 51478158), the New Century Excellent Talents in University (Project NCET-12-0838), the Fundamental Research Funds for the Central Universities of China (Grant No.PA2019GDZC0094) and the University collaborative innovation project in Anhui Province (Project GXXT-2019-005). The financial support is gratefully acknowledged. The authors also wish to thank the staffs at the Structures and Materials Laboratory of HFUT for their assistance.

Funding All persons who have made substantial contributions to the work reported in the manuscript, including those who provided editing and writing assistance but who are not authors, are named in the Acknowledgments section of the manuscript and have given their written permission to be named.

Compliance with ethical standards

Conflict of interest The authors declared that they have no conflicts of interest to this work.

Ethical statement I agree to be accountable for all aspects of the research in ensuring that all provided data and results are actual without academic fraud. I also promise that there will be no more submissions for one draft in this paper.

References

1. Annual Report on Prevention and Control of Solid Waste in China's Large and Medium-Sized Cities. https://www.sohu.com/a/209141737_682451.
2. Gomes R, Silvestre JD, de Brito J. Environmental life cycle assessment of the manufacture of EPS granulates, lightweight concrete with EPS and high-density EPS boards. *Journal of Building Engineering*. 2020;28:101031.
3. J. Daniel Ronald Joseph, J. Prabakar, P. Alagusundaramoorthy, Experimental studies on through-thickness shear behavior of EPS based precast concrete sandwich panels with truss shear connectors, *Composites Part B*.166 (2019) 446-456.
4. Mousavi SA, Zahrai SM, Bahrami-Rad A. Quasistatic cyclic tests on super-lightweight EPS concrete shear walls. *Eng Struct*. 2014;65:62–75.
5. S. Wu, W.L. Wang, C.Z. Ren, X.L. Yao, Y.G. Yao, Q.S. Zhang, Z.F. Li, Calcination of calcium sulphoaluminate cement using flue gas desulfurization gypsum as whole calcium oxide source, *Construction and Building Materials*. 228 (2019) 116676.A.
6. Zhang YJ, Pan F, Wu R. Study on the performance of FGD gypsum-metakaolin-cement composite cementitious system. *Constr Build Mater*. 2016;128:1–11.
7. Ye JH, Feng RQ, Chen W, Liu W. Behavior of cold-formed steel wall stud with sheathing subjected to compression. *J Constr Steel Res*. 2016;116:79–91.
8. Schafer BW, Ayhan D, Leng J, Liu P, Padilla-Llano D, Peterman KD, Stehman M, Buonopane SG, Eatherton M, Madsen R, Manley B, Moen CD, Nakata N, Rogers C, Yu C. Seismic response and engineering of cold-formed steel framed buildings. *Structures*. 2016;8:197–212.
9. Chen W, Ye JH, Bai Y, Zhao XL. Full-scale fire experiments on load-bearing cold-formed steel walls lined with different panels. *J Constr Steel Res*. 2012;79:242–54.
10. Kim T, Wilcoski J, Foutch DA, Lee MS. Shake table tests of a cold-formed steel shear panel. *Eng Struct*. 2006;28(10):1462–70.
11. Formisano A, Mazzolani FM, De Matteis G. Numerical analysis of slender steel shear panels for assessing design formulas. *Int J Struct Stab Dyn*. 2007;7(2):273–94.
12. Wang JF, Wang WQ, Xiao YM, Yu B. Cyclic test and numerical analytical assessment of cold-formed thin-walled steel shear walls using tube truss. *Thin-Walled Structures*. 2019;134:442–59.
13. K.D. Peterman, M.J.J. Stehman, R.L. Madsen, S.G. Buonopane, N. Nakata, B.W. Schafer, Experimental seismic response of a full-scale cold-formed steel-framed building. II: subsystem-level response, *Journal of Structural Engineering*. 142 (2016) 4016127.
14. Hegyi Péter, Dunai László. Experimental investigations on ultra-lightweight concrete encased cold-formed steel structures Part II: stability behavior of elements subjected to compression. *Thin-Walled Structures*. 2016;101:100–8.
15. Prabha P, Marimuthu V, Saravanan M, Palani GS, Lakshmanan N. Effect of confinement on steel-concrete composite lightweight load-bearing wall panels under compression. *J Constr Steel Res*. 2013;81:11–9.
16. Xu ZF, Chen ZF, Yang SH. Effect of a new type of high-strength lightweight foamed concrete on seismic performance of cold-formed steel shear walls. *Constr Build Mater*. 2018;181:287–300.
17. Wu HH, Chao SS, Zhou TH, Liu XB. Cold-formed steel framing walls with infilled lightweight FGD gypsum Part I: cyclic loading tests. *Thin-Walled Structures*. 2018;132:759–70.
18. J.V. Tapia, The development of novel infill materials for composite structural assemblies (Master thesis), Auckland University of Technology (AUT), 2013.
19. JGJ/T 70-2009, Standard for test method of performance on building mortar, Architecture & Industry Press of China, Beijing, 2009 (in Chinese).
20. GB/T 10294-2008, Thermal Insulation-Determination of Steady-State Thermal Resistance and Related Properties-Guarded Hot Plate Apparatus, Architecture & Industry Press of China, Beijing, 2008 (in Chinese).

21. JG/T 266-2011, Foamed concrete, Architecture & Industry Press of China, Beijing, 2011 (in Chinese).
22. Oluokun F. Prediction of concrete tensile strength from its compressive strength: an evaluation of existing relations for normal weight concrete. *ACI Mater J.* 1991;88(3):302–9.
23. C.E.B.F.I.P. MC90, Design of Concrete Structures. CEB-FIP Model Code 1990, Thomas Telford, London, 1993.
24. GB/T 50081-2019, Standard for test method of mechanical properties on ordinary concrete, Architecture & Industry Press of China, Beijing, 2019 (in Chinese).
25. Y.H. Mughahed Amran, Nima Farzadnia, A.A. Abang Ali, Properties and applications of foamed concrete: a review, *Constr. Build. Mater.* 101 (2015) 990-1005.
26. Mohebbi S, Mirghaderi SR, Farahbod F, Sabbagh AB, Torabian S. Experiments on seismic behaviour of steel sheathed cold-formed steel shear walls clad by gypsum and fiber cement boards. *Thin-Walled Structures.* 2016;104:238–47.
27. Pan CL, Shan MY. Monotonic shear tests of cold-formed steel wall frames with sheathing. *Thin-Walled Structures.* 2011;49:363–70.
28. JGJ 227-2011, Technical Specification for Low-rise Cold-formed Thin-walled Steel Building, Architecture & Industry Press of China, Beijing, 2011 (in Chinese).
29. AISI S213, North American Standard for Cold-formed Steel Framing-Lateral Design, American Iron and Steel Institute (AISI), Washington, DC, USA, 2007.
30. GB/T 15856.1-2002, Drilling Screws with Tapping Screw Thread, Standard Press of China, Beijing, 2002 (in Chinese).
31. GB/T 17657-2013, Test methods of evaluating the properties of wood-based panels and surface decorated wood-based panels, Architecture & Industry Press of China, Beijing, 2013 (in Chinese).
32. ATC-24, Guidelines for cyclic seismic testing of components of steel structures. Redwood City (CA): Applied Technology Council; 1992.
33. JGJ/T 101-2015, Specification for seismic test of building, General Administration of Quality Supervision, Inspection and Quarantine of PR China, Beijing, 2015 (in Chinese).
34. Design guide for light gauge steel buildings. Japan Iron and Steel Federation. Tokyo: Gihodo Shuppan Co., Ltd.; 2002 (**in Japanese**).
35. Hwang SJ, Lee HJ. Analytical model for predicting shear strengths of exterior reinforced concrete beam-column joints for seismic resistance. *Aci Structural Journal.* 1996;5:846–57.
36. Hwang SJ, Fang WH, Lee HJ, Yu HW. Analytical model for predicting shear strength of squat walls. *J Struct Eng.* 2001;127(1):43–50.
37. Hwang SJ, Lee HJ. Strength prediction for discontinuity regions by softened strut-and-tie model. *J Struct Eng.* 2002;128(12):1519–26.
38. Ye JH, Wang XX, Jia HY, Zhao MY. Cyclic performance of cold-formed steel shear walls sheathed with double-layer wallboards on both sides. *Thin-Walled Structures.* 2015;92:146–59.

Publisher's Note Springer Nature remains neutral with regard to jurisdictional claims in published maps and institutional affiliations.